Analysis of the photoconduction in CaF_2:Eu^{2+} crystals using the microwave resonant cavity technique

H. Loudyi,[1] Y. Guyot,[1,*] S. A. Kazanskii,[2] J.-C. Gâcon,[1] B. Moine,[1] C. Pédrini,[1] and M.-F. Joubert[1]

[1]*Université de Lyon, Université Lyon 1, CNRS, UMR 5620, Laboratoire de Physico-Chimie des Matériaux Luminescents, F-69622 Villeurbanne Cedex, France*

[2]*Center of Information Processing and Optical Technology, Saint-Petersburg State University of Information Technologies, Mechanics and Optics, Saint-Petersburg 197101, Russia*

(Received 29 November 2007; published 21 July 2008)

The microwave resonant cavity technique (MRCT) was used to measure the room-temperature photoconductivity spectrum of a CaF_2:Eu^{2+} single crystal between 275 and 450 nm, with the aim of positioning the Eu^{2+} levels relatively to the bottom of the host conduction band. A photoconductivity signal was detected at laser wavelengths $\lambda_l \leq 430$ nm ($h\nu_l \geq 2.9$ eV). Its intensity was observed to exhibit a superlinear dependence on the laser mean power for $\lambda_l > 280$ nm and an almost linear one at shorter wavelengths, showing that Eu^{2+} photoionization may involve either a one-photon or a two-step two-photon absorption process. The probabilities of both linear and quadratic processes were determined from measurements of the dependences of the photoconductivity signal intensity versus the mean laser power for several laser wavelengths within the spectral range that is under investigation. The Eu^{2+} photoionization threshold was estimated at 4.9 eV from the comparison between the MRCT photoconductivity spectrum, the Eu^{2+} $4f^6 5d(e_g)$ excited-state absorption spectrum, and the calculated density of states of the CaF_2 conduction band. In addition, the photoconduction dynamics in two CaF_2:Eu^{2+} samples grown under different experimental conditions was studied. The MRCT signals from the two samples were observed to exhibit different thermal behaviors. This observation is interpreted in terms of differences in trap densities and depths, in connection with thermoluminescence measurements.

DOI: 10.1103/PhysRevB.78.045111 PACS number(s): 78.47.−p, 78.70.Gq, 72.20.Jv, 78.55.Hx

I. INTRODUCTION

Microwave measurements of photoconductivity were previously performed in semiconductors.[1–4] Since photoconductivity signals in dielectric crystals are expected to be considerably smaller than those in semiconductors, a highly sensitive technique had to be developed for studying photoconductivity in insulating materials. As a matter of fact, we could observe photoconductivity signals in various rare-earth (RE) doped dielectric crystals using the microwave resonant cavity technique (MRCT) (Refs. 5–8). This technique consists of detecting the changes of the quality factor and resonant frequency of a microwave cavity resulting from pulsed-laser irradiation of a sample placed inside this resonator. In other words, MRCT looks at the perturbation of the microwave field inside the cavity induced by the interaction between the sample and the laser electromagnetic field. The various potentialities of MRCT were recently reviewed.[9] MRCT was also successfully applied to powdered samples of insulating materials with grain diameters ranging from 1–5 μm (Ref. 10). The primary goal of these investigations was indeed the location of the RE-ion energy levels within the host forbidden band gap via the determination of RE photoionization thresholds using a pulsed tunable dye laser for irradiation of the sample. Photoconductivity spectra could be measured by tuning the laser wavelength over a large spectral domain. Moreover, the dynamics of photoconduction could also be analyzed by taking advantage of the short laser-pulse duration (10 ns).

The present paper reports new MRCT measurements on two CaF_2:Eu^{2+} crystals grown under different experimental conditions. The CaF_2:Eu^{2+} photoconductivity spectrum is analyzed between 275 and 450 nm with a view to locating the position of the Eu^{2+} levels with respect to the CaF_2 conduction band (CB). In addition, information concerning the photoconduction dynamics and the effects of traps is obtained. Experimental details are given in Sec. II. Section III is devoted to the description and discussion of the experimental results. Concluding remarks are presented in Sec. IV.

II. EXPERIMENT

A. Materials

Two CaF_2:Eu^{2+} crystals originating from two different laboratories were studied. Samples 1 and 2 were grown by the Bridgman and Czochralski techniques in the Chemical Physics Department of the University of Geneva and the Vavilov State Optical Institute at Saint-Petersburg. The Eu^{2+} concentrations in samples 1 and 2 were estimated from absorption measurements to be at 9×10^{-3} and 1×10^{-3} mol %, respectively. Moreover, an undoped CaF_2 crystal was grown by the Bridgman technique. The crystals were cut and polished with random crystallographic orientation to cylindrical shape of diameter $\cong 2.5$ mm and height ranging from 2.5–6 mm, in order to fit in the microwave cavity. Square plates of $2 \times 2 \times 0.5$ mm^3 were also cut for thermoluminescence measurements.

B. Microwave setup

The microwave setup used for MRCT measurements was built on the basis of high-sensitivity microwave measuring

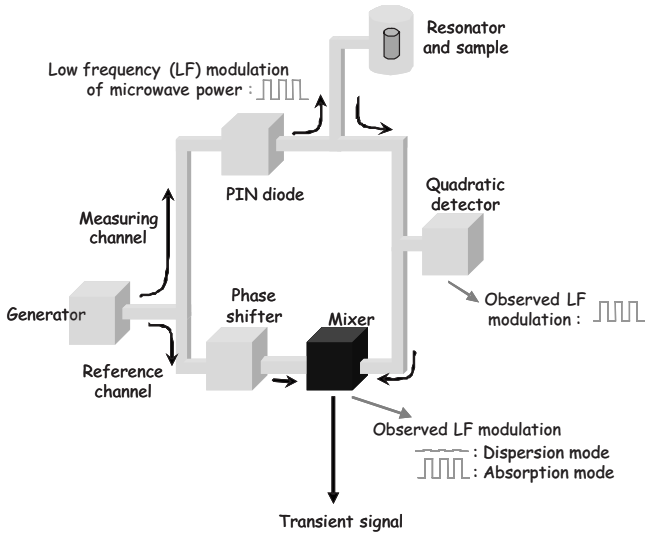

FIG. 1. Diagram of the microwave setup.

channels of electronic paramagnetic resonance spectrometers.[5,6] Improvements were progressively made in order to enhance the sensitivity. In addition, the setup was modified to offer the possibility of setting the temperature of the sample inside the cavity at any value between 5 and 300 K (Ref. 8). The scheme of the present setup is shown in Fig. 1. Technical details concerning the different components are given in previous papers.[5–8] The microwave bridge consists of a measuring channel containing the cylindrical reflex resonator with the sample inside and a reference one. Both channels end at a mixer diode that acts as a lock-in detector for recording weak microwaves reflected from the resonator that are in phase with microwaves propagating in the reference channel. As a consequence, the signal at the output of the mixer depends on the phase of the microwaves in the reference channel, which can be adjusted with a phase shifter. Cavity quality factor and resonance-frequency changes yield signals in absorption and dispersion modes, respectively.[6] Depending on the adjustment of the phase shifter in the reference channel, it is possible to get the microwave signal in either absorption, dispersion, or mixed mode. In fact, "pure" absorption or dispersion-mode signals are much sought after, since they are connected with conduction or trapped electrons, respectively.[1]

In order to accurately adjust the phase shifter for measuring pure mode signals, the microwave power in the measuring channel is modulated by a ~1 kHz square-wave voltage, thanks to a *p-i-n* diode controlled microwave attenuator. A part of the resulting signal at the output of the mixer is then amplified in a low-frequency amplifier allowing the observation of a square-wave signal, the height of which depends on the adjustment of the phase shifter. This height is minimum when tuning in dispersion mode, since the dispersion-mode signal vanishes when the microwave frequency coincides with the cavity resonance frequency.[6] On the other hand, adjusting the phase shifter so that this height reaches a maximum ensures tuning in absorption mode. The accuracy of this procedure was estimated to be around 90% (Ref. 8). The modulation voltage was indeed switched off during the MRCT measurement itself.

C. Optical setup

The lower part of the sample was uniformly irradiated by the frequency-doubled output beam from a pulsed YAG: Nd-pumped tunable dye laser. BBO and KDP crystals were used for frequency doubling. No less than eight dye solutions were required to cover the 275–450 nm spectral range. The MRCT photoconductivity spectrum was obtained by measuring the intensity (averaged out over 300 laser pulses) of the microwave signal in absorption mode for each laser wavelength. This intensity is proportional to the mean number of photons absorbed per second in the material i.e., to both the absorption rate A and laser wavelength λ_l, if the laser energy per pulse is maintained at a constant value for each measurement (around 360 μJ). The intensity of the microwave signal in absorption mode was therefore divided by λ_l times A, in order to ensure that each measurement refers to the same number of photons absorbed in the sample.

D. Thermoluminescence measurements

The samples were cooled to 105 K and irradiated with the 193 nm (6.4 eV) line of a pulsed ArF laser for a few minutes (pulse duration 5 ns, repetition rate 20 Hz, and maximum energy per pulse 50 μJ). This excitation merely promotes Eu^{2+} ions into $4f^6 5d(t_{2g})$ states, since the charge-transfer band is located at 8.2 eV (Ref. 11) and the CaF_2 forbidden band gap is about 12 eV (Ref. 12). Efficient transitions from $4f^6 5d(t_{2g})$ states to CB states may then take place. Heating the samples up to 700 K at a constant rate of 10 K/min results in emptying the electron traps and the released electrons may then recombine with Eu^{3+} ions, which are intrinsically present in the sample or result from Eu^{2+} ionization, giving rise to the blue Eu^{2+} luminescence that is detected during the heating ramp.

III. RESULTS AND DISCUSSION

Typical room-temperature one-photon absorption and emission spectra for $CaF_2:Eu^{2+}$ (sample 1) are shown in Fig. 2. The observed bands are attributed to parity-allowed electric-dipole transitions between $4f^7$ and $4f^6 5d$ states. Due to substitution of Eu^{2+} ions at Ca^{2+} sites of O_h symmetry, the $5d$ electron orbital splits into e_g and t_{2g} components. As a consequence, the $4f^6 5d$ configuration appears to be composed of two well-separated groups of levels, which may be labeled as e_g and t_{2g} groups. Hence, the two groups of bands observed in the absorption spectrum between 300 and 420 nm, on one hand, and below 300 nm, on the other hand, originate from $4f^7(^8S_{7/2}) \rightarrow 4f^6 5d(e_g)$ and $4f^7(^8S_{7/2}) \rightarrow 4f^6 5d(t_{2g})$ transitions, respectively. The emission spectrum in Fig. 2 was obtained under excitation at 284 nm. It exhibits a band peaking around 425 nm, originating from $4f^6 5d(e_g) \rightarrow 4f^7$ transitions with a decay time around 0.7 μs. The lowest $4f^6 5d(e_g)$ level may be located at 3 eV above the $4f^7(^8S_{7/2})$ ground level from the absorption and emission spectra shown in Fig. 2.

The photoconductivity spectrum (sample 1) obtained from MRCT measurements is shown in Fig. 3 with the one-photon absorption spectrum for the purpose of comparison. Note

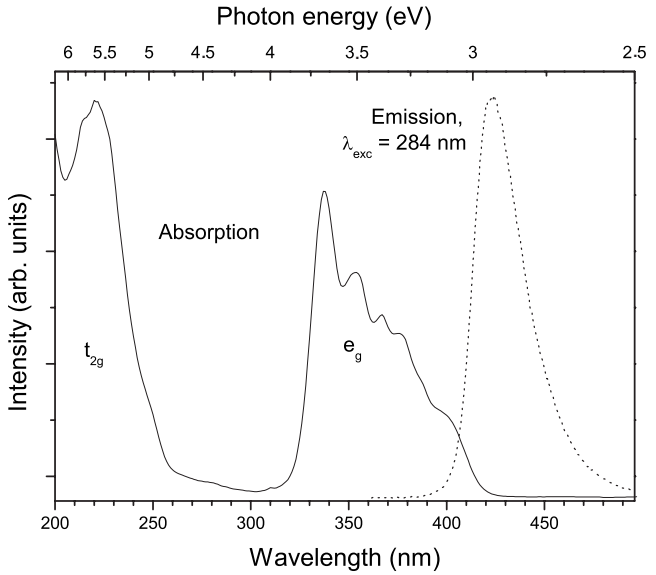

FIG. 2. Room-temperature absorption and emission spectra of $CaF_2:Eu^{2+}$ (sample 1).

that the shapes of the absorption spectra in Figs. 2 and 3 differ, since they refer to the optical density and the absorption percentage, respectively. Of course, it was checked that no signal was detected for the undoped CaF_2 sample even for laser energies as high as 1 mJ/pulse. From the spectra displayed in Fig. 3, one can first conclude that photoconduction takes place within the Eu^{2+} $4f^7(^8S_{7/2}) \rightarrow 4f^6 5d$ band domain. Hence, Eu^{2+} photoionization involves transitions toward $4f^6 5d$ states as the first step. At this point, it is worth remembering that the intensity of the $CaF_2:Eu^{2+}$ MRCT signal was previously shown to exhibit a superlinear dependence on the energy per laser pulse E_{exc} at $\lambda_l = 355$ nm (3.5 eV), indicating that absorption in the $4f^6 5d$ excited state takes place under these experimental conditions.[6] Such an excited-state absorption (ESA) process should obviously be involved in the Eu^{2+} photoionization under excitation at $\lambda_l > 355$ nm. As a consequence, measurements of the dependency of the

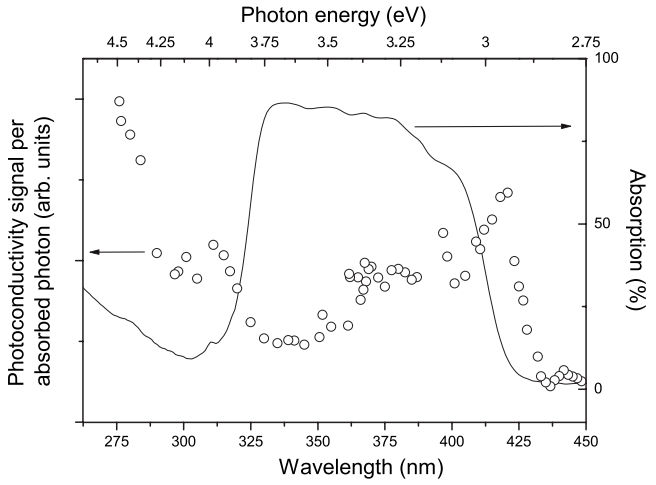

FIG. 3. Comparison between room-temperature photoconductivity and absorption spectra of $CaF_2:Eu^{2+}$ (sample 1).

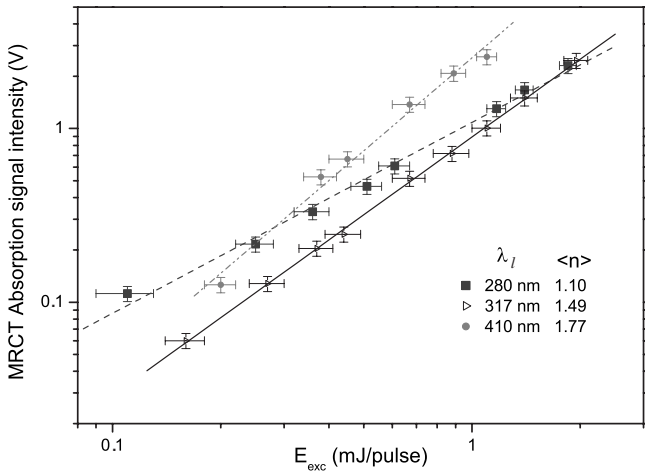

FIG. 4. MRCT signal intensity dependence on the energy per laser pulse (E_{exc}) at laser wavelengths $\lambda_l = 280$, 317, and 410 nm.

MRCT signal intensity on E_{exc} proved to be essential for interpreting the photoconductivity spectrum. This dependency was measured for 11 values of the excitation wavelength within the 275–440 nm domain. As a result, the MRCT signal intensity was observed to be proportional to $(E_{exc})^{\langle n \rangle}$, with $\langle n \rangle$ increasing continuously from 1.1 to 1.8 as the wavelength is increased (see Fig. 4). Obviously, $\langle n \rangle$ may be interpreted as the mean number of photons required to ensure Eu^{2+} photoionization for a given excitation wavelength. Since the photoionization process should involve either one-photon or two-step two-photon excitation, $\langle n \rangle$ may also be expressed in terms of the probabilities p_1 and p_2 for the linear and quadratic processes under consideration.

$$\langle n \rangle = \sum_{n=1}^{2} n p_n = p_1 + 2p_2 = 1 + p_2 = 2 - p_1, \qquad (1)$$

since

$$p_1 + p_2 = 1. \qquad (2)$$

The experimental dependences of p_1 and p_2 versus the laser photon energy $E = h\nu_l$ are displayed on Fig. 5. They would be expected to behave like Heaviside step functions jumping from 0 to 1 around a threshold energy E_0 corresponding to the one-step Eu^{2+} photoionization threshold. In fact, p_1 and p_2 exhibit much smoother dependences on E. As a consequence, the one-step Eu^{2+} photoionization threshold cannot be directly obtained from the data displayed in Fig. 5. However, it is to be noted that the linear process (probability p_1) appears to predominate over the quadratic one (probability p_2) for the highest energy value $E \cong 4.5$ eV only. The one-step Eu^{2+} photoionization threshold should therefore be at least equal to this value or even higher.

Since ESA within the $4f^7(^8S_{7/2}) \rightarrow 4f^6 5d(e_g)$ band domain is involved in the Eu^{2+} photoionization process at low photon energy, it is worthwhile comparing the MRCT photoconductivity spectrum displayed in Fig. 3 with the e_g ESA spectrum in the spectral domain under consideration (see Fig. 6). This ESA spectrum was obtained by using the pump-probe technique with a pump laser at 355 nm promoting Eu^{2+} ions into

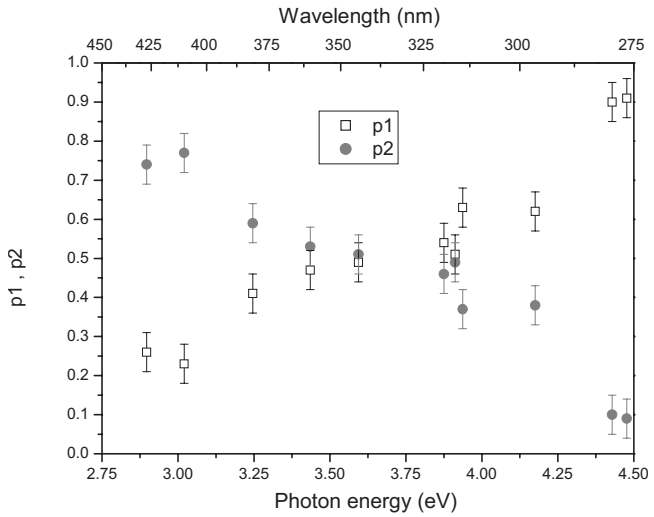

FIG. 5. Variations of the one-photon (p_1) and two-step two-photon (p_2) photoionization probabilities versus the laser photon energy (eV). These probabilities are determined to within an accuracy of 0.05.

a $4f^6 5d$ level at 3.5 eV above the $4f^7(^8S_{7/2})$ ground level.[13] Then these ions are expected to experience a nonradiative relaxation toward the lowest $4f^6 5d$ level lying at 3.0 eV above the Eu^{2+} ground level (see above). Comparing the MRCT and ESA spectra leads us to consider three distinct domains (see Fig. 6).

(i) In the 427–413 nm range (photon energy E between 2.9 and 3.0 eV), the MRCT signal increases first, reaches a maximum for $\lambda \cong 418$ nm, and then decreases, while the ESA spectrum exhibits a continuous decrease. Photoconduction mainly results from a two-step two-photon absorption in this spectral domain (see Fig. 5). As shown above, the initial state of ESA is located at 3.0 eV in both experiments, the energy mismatch being supplied by the lattice in the case of

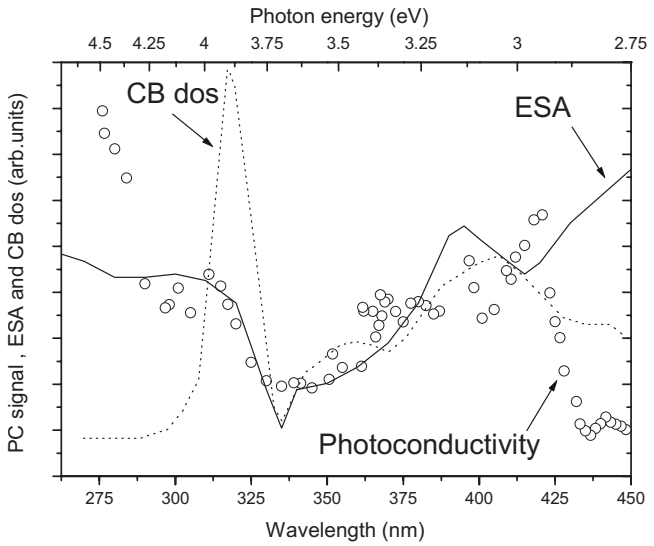

FIG. 6. $CaF_2:Eu^{2+}$ photoconductivity (Photoconductivity) and e_g excited-state absorption (ESA) spectra. CaF_2 conduction-band density of states (CB DOS). ESA and CB DOS data were obtained from Refs. 13 and 12, respectively.

MRCT measurements. Hence, the ESA final states should lie between 5.9 and 6 eV above the $4f^7(^8S_{7/2})$ ground level. It is clear, from the one-photon absorption spectrum in Fig. 2, that these states belong to the $4f^6 5d(t_{2g})$ group. Consequently, the photoconduction process is governed by a two-step autoionization process involving $4f^6 5d(t_{2g})$ states degenerated within the CB. The discrepancy initially observed between the ESA and photoconductivity spectra, most probably, originates from the fact that for ESA measurements, the excitation into the $4f^6 5d(e_g)$ level at 3.0 eV is efficiently achieved by the laser pump, whatever the wavelength of the probing source may be. While it is not the case for MRCT measurements, in which both the absorbed photons are issued from the same laser beam. Furthermore, annihilation of lattice phonons is required in the latter case.

(ii) In the 413–288 nm range ($3.0 < E < 4.3$ eV), both ESA and photoconductivity spectra remarkably match each other. Of course, the laser beam in the MRCT experiment efficiently populates the $4f^6 5d(e_g)$ level at 3.0 eV, as well as the laser pump does in ESA measurements. The ESA final states lie between 6.0 and 7.3 eV above the $4f^7(^8S_{7/2})$ ground level and the photoconduction process is also governed by a two-step autoionization process involving $4f^6 5d(t_{2g})$ states degenerated within the CB.

(iii) The photoconductivity spectrum increases much more than the ESA one with decreasing the laser wavelength below 288 nm ($E > 4.3$ eV). As the one-photon excitation predominates over the two-step two-photon excitation in MRCT measurements in this spectral domain (see Fig. 5), the photon energy should be high enough to ensure the promotion of Eu^{2+} ions in $4f^6 5d(t_{2g})$ states degenerated within the CB, with the energy mismatch being supplied by the lattice if necessary. This one-photon autoionization process is much more efficient than the two-step two-photon absorption involved in the ESA measurements, thus explaining the observed discrepancy between the MRCT photoconductivity and ESA spectra in this domain.

It should be noted now that an e_g ESA spectrum of similar shape, as the one shown in Fig. 6, was reported for $CaF_2:Sm^{2+}$, proving that the ESA final states are related with the CaF_2 host rather than the rare-earth ion.[14] Hence, the ESA spectrum should reflect the CaF_2 conduction-band density of states (CB DOS). Calculations of the CaF_2 CB structure were reported by Heaton *et al.*[12] The resulting calculated CB DOS may be easily brought into coincidence with the e_g ESA spectrum, as shown in Fig. 6, by adjusting its sharp minimum with the one located at $\lambda = 335$ nm (3.7 eV) in the e_g ESA spectrum. As this minimum is known to lie at 1.8 eV above the CB bottom (see Ref. 12), it is then possible to determine the position of the $4f^7(^8S_{7/2})$ ground level relative to the CB bottom as follows. The absorption of a 3.7 eV ($\lambda = 335$ nm) photon by Eu^{2+} ions in the lowest $4f^6 5d(e_g)$ excited state results in a transition toward the CB level lying at 1.8 eV above the CB bottom, on one hand, and at 6.7 eV above the $4f^7(^8S_{7/2})$ ground level, on the other hand. Hence, the Eu^{2+} ground level should lie at 4.9 eV under the CB bottom. This value is very close to the Eu^{2+} photoionization threshold calculated in the framework of an electrostatic model (4.86 eV) (Ref. 15). It is also in agreement with the data displayed in Fig. 5 (see above). An energy-level dia-

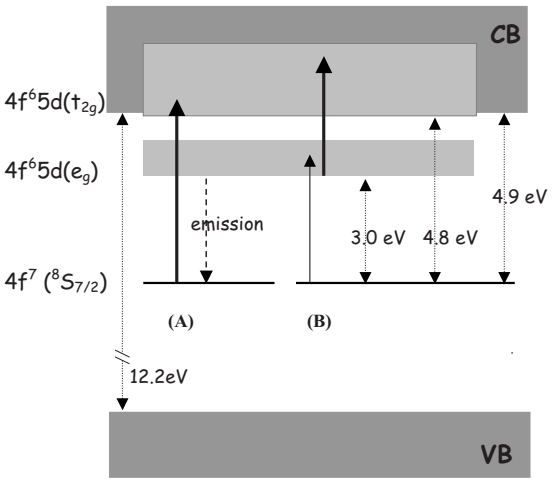

FIG. 7. Energy-level diagram showing the location of the Eu^{2+} levels with respect to the CaF_2 conduction band in CaF_2:Eu^{2+}. The absorption transitions involved in one- and two-step autoionization processes (labeled *A* and *B*, respectively) are shown by vertical arrows.

gram showing the location of the Eu^{2+} levels with respect to the CaF_2 CB may be drawn from the above discussion (see Fig. 7).

MRCT measurements also yield information concerning the dynamics of photoconduction.[9] Of course, the decay of the absorption mode signal reflects the decay of the CB electronic population. This decay originates from the capture of electrons by Eu^{3+} ions (either resulting from Eu^{2+} photoionization or initially present in the sample), but also by traps. Trapped electrons may return back to the CB, thanks to thermal activation. Thus, the successive CB→trap level→CB transitions contribute to increase the lifetime τ of mobile electrons in the CB. Since the probability for an electron to escape at temperature T from a trap of depth ΔE is proportional to $\exp(-\Delta E/kT)$, the electron will live on the trap during a time that increases as $\Delta E/kT$ increases. Hence, the temperature dependence of the full width at half maximum (FWHM) of the absorption mode signal, which turns out to be a measure of τ, should be affected by trapping effects. The thermal behaviors of τ for the two samples at our disposal were observed to differ significantly, especially at low temperatures (see Fig. 8). The observed lengthening of τ between 300 and 10 K is much more pronounced for sample 2 than for sample 1. Since trapping effects are suspected to play a role, thermoluminescence spectra were carried out in order to get information on the density and depth of traps in the two samples. In fact, the spectra of samples 1 and 2 also exhibit strong differences in the temperature range under investigation (see Fig. 9). Strong and broad thermoluminescence peaks are observed in the spectrum of sample 2 while none appears in the other one. The four main peaks in the spectrum of sample 2 occur at temperatures around 196, 249, 342, and 436 K. They correspond to electronic traps with respective mean depths estimated at 0.6, 0.9, 1.2, and 1.4 eV. Hence, the differences observed between the temperature dependences shown in Fig. 8 may be correlated with those appearing in the thermoluminescence spectra in Fig. 9 as

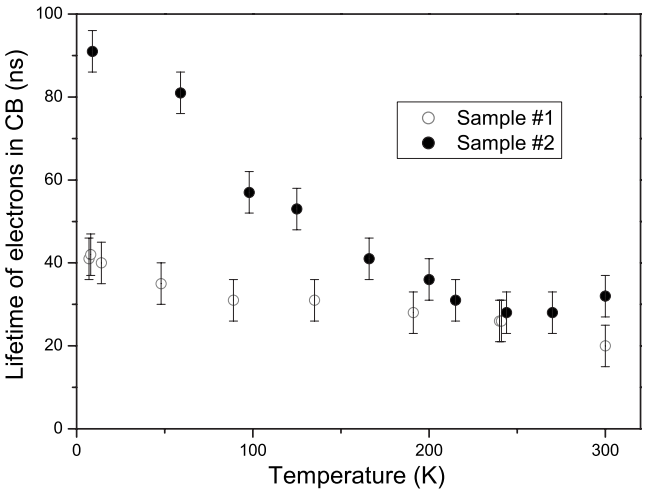

FIG. 8. Thermal behaviors of the lifetime τ of electrons released in the conduction band for CaF_2:Eu^{2+} samples 1 (o) and 2 (●). τ is determined to within an accuracy of 5 ns.

follows. As the temperature of sample 2 is lowered, τ experiences a significant lengthening due to the effects of the deep traps revealed by the thermoluminescence spectrum, while the absence of such deep traps in sample 1 results in an almost temperature independent lifetime of CB electrons above 90 K. The very moderate lengthening of τ, observed for sample 1 below 90 K, might originate from shallow traps, which could not be revealed by the thermoluminescence spectrum since our equipment did not allow measurements below 105 K.

IV. CONCLUSION

The CaF_2:Eu^{2+} photoconductivity spectrum was obtained from measurements of MRCT absorption mode signals at fixed laser wavelengths between 275 and 450 nm. As a first result, photoconduction was shown to take place within the domain of the Eu^{2+} $4f^7(^8S_{7/2})\rightarrow 4f^6 5d$ absorption bands. The

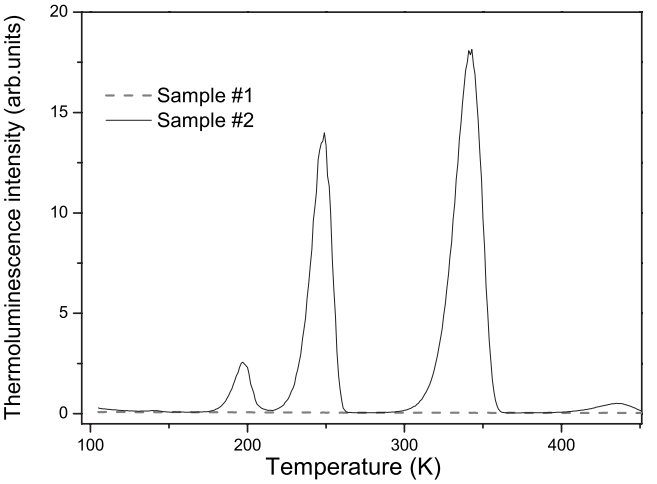

FIG. 9. Thermoluminescence spectra of CaF_2:Eu^{2+} samples 1 (dashed line) and 2 (continuous line).

Eu^{2+} photoionization threshold could not, however, be determined from the measured photoconductivity spectrum directly. In fact, the dependency of the MRCT signal intensity on the mean power of the pulsed laser was found to be superlinear at wavelengths higher than 280 nm, showing that photoconduction involves a two-step two-photon absorption process in this spectral domain. The mean number of photons required to ensure Eu^{2+} photoionization for a given excitation wavelength was shown to increase continuously from 1.1 to 1.8 as the laser wavelength is increased from 280 up to 410 nm, hence, reflecting the competition between a linear process and a quadratic one. Comparing the present photoconductivity spectrum with a previously published ESA spectrum in the domain of the $4f^7(^8S_{7/2}) \rightarrow 4f^6 5d(e_g)$ absorption bands led to the conclusion that photoconduction is governed in this spectral domain by a two-step autoionization process involving $4f^6 5d(t_{2g})$ states degenerated within the CB. Then a much more efficient one-step autoionization process takes place as soon as the photon energy is high enough to directly promote Eu^{2+} ions into these $4f^6 5d(t_{2g})$ states. The Eu^{2+} photoionization threshold was then estimated at 4.9 eV from the comparison between the MRCT photoconductivity spectrum, the ESA spectrum, and the calculated CaF_2 CB DOS. An energy-level diagram showing the location of the Eu^{2+} levels with respect to the CaF_2 CB was then proposed. In addition, MRCT was used to study the photoconduction dynamics. The lifetime τ of the CB electrons was measured from the FWHM absorption mode photoconductivity signal. Its thermal dependence was studied for two $CaF_2:Eu^{2+}$ crystals (samples 1 and 2) grown under different experimental conditions. The differences observed in the thermal behaviors of τ were attributed to trapping effects, since strong peaks associated to deep traps appear in the thermoluminescence spectrum of sample 2, while they are missing in the spectrum of sample 1. Hence, MRCT measurements may be useful to study the influence of traps on the recombination processes following photoionization.

*Author to whom correspondence should be addressed: Dr. Yannick Guyot, LPCML, bât. Alfred Kastler, 10, rue Ampère, Domaine Scientifique de la Doua, Université Claude Bernard Lyon1, 69622 Villeurbanne cedex, France. guyot@pcml.univ-lyon1.fr

[1] S. Grabtchak and M. Cocivera, Phys. Rev. B **58**, 4701 (1998).
[2] M. Ichimura, H. Taijiri, Y. Morita, N. Yamada, and A. Usami, Appl. Phys. Lett. **70**, 1745 (1997); M. Ichimura, N. Yamada, H. Taijiri, and E. Arai, J. Appl. Phys. **84**, 2727 (1998).
[3] S. V. Garnov, A. I. Ritus, S. M. Klimentov, S. M. Pimenov, V. I. Konov, S. Gloor, W. Lüthy, and H. P. Weber, Appl. Phys. Lett. **74**, 1731 (1999).
[4] S. A. Kazanskii, D. S. Rumyantsev, and A. I. Ryskin, Phys. Rev. B **65**, 165214 (2002).
[5] M.-F. Joubert, S. A. Kazanskii, Y. Guyot, J.-C. Gâcon, J.-Y. Rivoire, and C. Pédrini, Opt. Mater. (Amsterdam, Neth.) **24**, 137 (2003).
[6] M.-F. Joubert, S. A. Kazanskii, Y. Guyot, J.-C. Gâcon, and C. Pédrini, Phys. Rev. B **69**, 165217 (2004).
[7] Y. Guyot, H. Loudyi, S. A. Kazanskii, J.-C. Gâcon, C. Pédrini, and M.-F. Joubert, Radiat. Meas. **38**, 753 (2004).
[8] M.-F. Joubert, S. A. Kazanskii, Y. Guyot, H. Loudyi, J.-C. Gâcon, and C. Pédrini, Opt. Mater. (Amsterdam, Neth.) **28**, 35 (2006).
[9] H. Loudyi, Y. Guyot, S. A. Kazanskii, J.-C. Gâcon, C. Pédrini, and M.-F. Joubert, Phys. Status Solidi C **4**, 784 (2007).
[10] H. Loudyi, Y. Guyot, J.-C. Gâcon, C. Pédrini, and M.-F. Joubert, J. Lumin. **127**, 171 (2007).
[11] P. Dorenbos, J. Lumin. **111**, 89 (2005).
[12] R. A. Heaton and C. C. Lin, Phys. Rev. B **22**, 3629 (1980).
[13] J. K. Lawson and S. A. Payne, Phys. Rev. B **47**, 14003 (1993).
[14] J. K. Lawson and S. A. Payne, J. Opt. Soc. Am. B **8**, 1404 (1991).
[15] J. F. Owen, P. P. Dorain, and T. Kobayashi, J. Appl. Phys. **52**, 1216 (1981).